POLITECNICO DI TORINO
Repository ISTITUZIONALE

Bio-based cellulose-filled vitrimers for 3D printing via liquid deposition modeling: Rheological tuning and environmental assessment

Original
Bio-based cellulose-filled vitrimers for 3D printing via liquid deposition modeling: Rheological tuning and environmental assessment / Albertini, E., Busto, M., Dalle Vacche, S., Blengini, G.A., Guerre, M., Vitale, A.. - In: CHEMICAL ENGINEERING JOURNAL. - ISSN 1385-8947. - ELETTRONICO. - 528:(2026), pp. 1-12. [10.1016/j.cej.2025.172399]

Availability:
This version is available at: 11583/3006548 since: 2026-01-14T08:43:51Z

Publisher:
Elsevier

Published
DOI:10.1016/j.cej.2025.172399

Terms of use:

This article is made available under terms and conditions as specified in the corresponding bibliographic description in the repository

Publisher copyright

(Article begins on next page)

26 November 2026

Chemical Engineering Journal 528 (2026) 172399

Contents lists available at ScienceDirect

Chemical Engineering Journal

journal homepage: www.elsevier.com/locate/cej

Bio-based cellulose-filled vitrimers for 3D printing via liquid deposition modeling: Rheological tuning and environmental assessment

Edoardo Albertini [a], Mirko Busto [a], Sara Dalle Vacche [a], Gian Andrea Blengini [a], Marc Guerre [b,*], Alessandra Vitale [a,*]

[a] Politecnico di Torino, Corso Duca degli Abruzzi 24, 10129, Turin, Italy
[b] Laboratoire Softmat, CNRS UMR 5623, Université de Toulouse, Université Paul Sabatier, 118 Route de Narbonne, 31062, Toulouse, Cedex 9, France

ARTICLE INFO

Keywords:
Disulfide vitrimer
Bio-based vitrimer
Sustainable epoxy composites
LDM
Life cycle assessment

ABSTRACT

To address the need for sustainable materials in 3D printing applications, a bio-based vitrimer was developed using an epoxy resin derived from cardanol and cystamine as a cross-linker. Cystamine was chosen due to its dynamic disulfide bonds, bio-based nature and highly reactive aliphatic amine groups, enabling rapid network formation under mild thermal conditions. Microfibrillated cellulose (MFC) and ultrafine cellulose (UFC) were used as bio-based fillers and rheology modifiers to formulate printable pastes. The curing process was thoroughly investigated by DSC and FTIR-ATR, confirming efficient cross-linking under the selected conditions. Thermal and structural properties of the vitrimers were characterized by gel content, swelling, and heat resistance analyses. The printability of the pastes via Liquid Deposition Modeling was evaluated through rheological analysis, and a concentration of 13 wt% MFC and 13 wt% UFC was identified as the optimal compromise between shear-flow behavior and post-print structural integrity. Simple and more complex geometries were printed and then cured at 30–80 °C, ensuring high shape fidelity (87.0 %). The vitrimer behavior was confirmed by stress-relaxation experiments, showing an overall activation energy in the range of 63–65 kJ mol^{-1}, and by successful mechanical recyclability. Finally, a preliminary Life Cycle Assessment underscored the potential of these materials for sustainable additive manufacturing.

1. Introduction

Liquid Deposition Modeling (LDM) is a recent 3D printing technique similar to Direct Ink Writing (DIW) and Fused Deposition Modeling (FDM). It involves three main steps: extrusion of a paste or gel using a syringe or screw extruder, layer-by-layer deposition and solidification (through evaporation, gelation, or cross-linking) [1–4]. In LDM, one or more fillers are incorporated into a liquid phase (i.e., a reactive resin or a solvent) to produce shear-thinning fluids characterized by a yield stress [5–7]. These fluids do not flow unless the applied stress exceeds the yield stress, and during flow, their apparent viscosity decreases with increasing shear rate. This rheological behavior enables the material to act as a solid when printed, yet to flow like a liquid during extrusion [8,9]. In recent years, LDM has been increasingly applied to various materials, particularly ceramic and polymer-based pastes. However, studies specifically addressing epoxy thermosets remain scarce, and only a few examples of LDM-processed epoxy vitrimers have been reported in the literature [10,11].

Epoxy thermosets, with their cross-linked structure, are of particular interest for 3D printing applications due to their superior chemical and mechanical resistance compared to conventional thermoplastics [12]. However, their limited reprocessability at end-of-life, combined with the need for high-temperature curing—which poses a risk of significant deformation and collapse during final curing—has severely limited their use for 3D printing. Beyond that, increasingly stringent regulations on fossil-derived raw materials for epoxy resins (i.e., bisphenol A and epichlorohydrin) further limit their adoption in new applications [13,14]. To solve both these problems, in this work, a fully bio-based epoxy vitrimer able to cross-link at low temperatures and showing reprocessability was developed starting from a bio-based resin (Cardolite® LITE 514HP, hereafter named 514HP), ultrafine cellulose (UFC) and microfibrillated cellulose (MFC) as fillers, and a dynamic diamine hardener containing disulfide bonds (cystamine).

514HP is a flexible epoxy resin produced by epoxidation of cardanol

* Corresponding authors.
E-mail addresses: marc.guerre@cnrs.fr (M. Guerre), alessandra.vitale@polito.it (A. Vitale).

https://doi.org/10.1016/j.cej.2025.172399
Received 12 September 2025; Received in revised form 16 December 2025; Accepted 27 December 2025
Available online 29 December 2025
1385-8947/© 2026 The Authors. Published by Elsevier B.V. This is an open access article under the CC BY license (http://creativecommons.org/licenses/by/4.0/).

Table 1
Investigated formulations and characterization of the cured samples: fillers amount, conversion α, gel content, swelling values, T_g and $T_{5\%}$ of cross-linked samples.

	MFC [wt%]	UFC [wt%]	α [%]	Gel content [%]	$Swelling_{dry}$ [a] [%]	$Swelling_0$ [b] [%]	T_g [°C]	$T_{5\%}$ [°C]
NoFiller	–	–	100	98.9 ± 0.1	1.8 ± 0.0	1.0 ± 0.0	23	257
13UFC	–	13	94	99.9 ± 0.0	5.7 ± 0.3	4.5 ± 0.3	18	265
13MFC	13	–	95 (bottom) – 83 (top)	80.8 ± 0.2	24.8 ± 1.0	10.2 ± 4.9	16	194
13MFC + 9UFC	13	9	95	82.1 ± 0.4	27.2 ± 0.1	11.7 ± 0.0	16	199
13MFC + 11UFC	13	11	92	83.2 ± 0.0	29.5 ± 0.3	10.1 ± 0.0	17	201
13MFC + 13UFC	13	13	94	82.8 ± 0.0	28.9 ± 0.1	13.9 ± 0.9	15	204

[a] m_0 is taken after swelling and drying.
[b] m_0 is taken before immersing the samples in water.

extracted from purified raw cashew nutshell liquid (CNSL) [15,16]. Epoxy thermosets produced from cardanol derivatives, both as cross-linkers or epoxy resins, have been studied in recent years and have recently found application in several fields [17–19]. However, only a few works have reported cardanol-based vitrimers [20], and applications of such systems in LDM remain very limited. Apart from the study of Capannelli et al. [11], which demonstrated cardanol-based vitrimers for LDM via transesterification at elevated temperature, the combination of bio-derived epoxy resins, mild-temperature curing without catalysts, dynamic disulfide exchange, and LDM processing remains unexplored.

Cystamine is an aliphatic diamine containing a disulfide bond derived from an amino acid. Its dynamic behavior has recently been studied, demonstrating the molecule's ability to undergo disulfide exchange reactions [21,22]. This hardener has been combined with epoxy resins to produce vitrimers that can be reshaped and reprocessed at high temperatures, above their glass transition. These characteristics of reprocessing and reshaping contribute to the environmental sustainability of the resulting materials [23], showing significant potential for advanced manufacturing applications in areas such as electronics, automotive, and biomedical devices [24]. Moreover, they have recently gained interest in the 3D printing sector [25,26]. In this work, cystamine was employed as a curing agent due to its advantageous properties, including a liquid state, low viscosity, and catalyst-free reactivity nature. These properties enable efficient mixing with high filler contents, which is crucial for LDM applications [3]. Furthermore, its ability to start the cross-linking reaction with epoxy resins at quite low temperatures (i.e., above 30 °C) helps in preserving the shape of the 3D printed piece during the initial curing stage. Then, a complete cross-linking can be subsequently achieved via a second curing step at slightly higher temperature (i.e., 80 °C). This approach represents a unique advancement in the field of 3D printing, as it combines bio-based materials with the innovative use of epoxy vitrimers for LDM, enabling low-temperature, catalyst-free curing, reshaping, and reprocessing without compromising the mechanical stability of the printed structures.

Fillers are the most important part of polymeric pastes for LDM: their addition to the thermoset polymer causes a radical change in the rheological properties of the fluid making it suitable for 3D printing [27–29]. Cellulose is the most common biopolymer highly present in nature and it can be utilized to make bio-composites and 3D printable pastes [30]. However, the hydrophilic nature of cellulose represents a disadvantage to its application due to the difficulty of homogeneous dispersion in most non-polar polymer matrices [31,32]. Cellulose can be extracted through mechanical, chemical, or enzymatic treatments from different sources such as plants, algae, bacteria and tunicates [33,34]. Ultrafine cellulose (UFC) and microfibrillated cellulose (MFC) were used together as fillers in this work. UFC refers to cellulose particles with sizes in the range of few micrometers. MFC is instead more uniform and nanoscaled; it is obtained through a simple mechanical process that includes refining and high-pressure homogenization [35,36]. This process applies mechanical shear forces that promote the fibrillation of cellulose fibers, producing microfibrils with diameters between 10 and 100 nm and lengths in the micrometer range [37–39].

To select the most appropriate formulation, the influence of the used fillers on the cross-linking reaction, rheology properties and dynamic bond exchange of the prepared pastes was also deeply investigated. Mechanical reshaping was successfully performed and finally, the formulation with the highest amount of fillers was 3D printed. A Life Cycle Assessment (LCA) was performed to evaluate the environmental performance of vitrimer production at the laboratory scale, following the European Commission's guidelines and reports [40–42], and ISO standards as references [43,44].

2. Experimental section

2.1. Materials

The cardanol-based epoxy resin Cardolite® LITE 514HP (514HP), with an epoxide equivalent weight (EEW) of 302 g/eq and a viscosity of 5790 cps was supplied by Cardolite® Corporation. Cystamine dihydrochloride 96 %, methanol 99.9 %, acetonitrile 99.9 %, potassium hydroxide and magnesium sulfate anhydrous were all purchased from Sigma Aldrich. Two cellulosic fillers were used in this work: microfibrillated cellulose Celova® MFC Powder (MFC), a powder with 40–60 wt% MFC content with a residual moisture less than 10 %, purchased from Weidman, and ultrafine cellulose dry powder Technocel® FM8 (UFC) supplied by CFF GmbH & Co. KG, with a particle diameter of 6–12 μm and a length of 9–10 μm. 514HP, MFC and UFC were used as received.

2.2. Cystamine desalination

To prepare 5 g of desalinated cystamine (cys), 7.4 g of cystamine dihydrochloride were dissolved in 350 mL of methanol. Separately, 3.7 g of KOH were dissolved in 50 mL of methanol. After 1 h, the KOH solution was added to the cystamine solution and stirred for another hour. The formed KCl was removed by filtration, methanol was evaporated using an evaporator and residue was dried over $MgSO_4$ in acetonitrile. After complete evaporation of acetonitrile, the cystamine was obtained as a yellowish liquid and stored at 3–4 °C. The cystamine desalination process was carried out at room temperature. The recovery rates of methanol and acetonitrile were verified by volume measurements. The ^1H NMR spectrum of cystamine and the reaction scheme for the desalination process are reported in Fig. S1 of the Supporting Information.

2.3. Preparation of vitrimer formulations

Formulations containing 514HP and cystamine with 1.2 equivalent of curing agent were prepared via mixing with a speed mixer DAC 250.3 FVZ (Hauschild) at 2000 rpm for 2 min. The amount of cystamine in the formulations was calculated from the epoxide equivalent weight (EEW = 302 g/eq) and amine hydrogen equivalent weight (AHEW = 38 g/eq), according to Eq. 1:

$$phr_{cystamine} = (AHEW/EEW) \times 1.2 \times 100 \quad (1)$$

where $phr_{cystamine}$ corresponds to the amount of hardener to add for 100

g of epoxy resin. TGA analysis revealed that the MFC powder contained approximately 10 wt% of water and ≈ 45 wt% of glycerol (see Fig. S2 of the Supporting Information) [45,46], consistent with the information reported in the Technical Datasheet. Since glycerol is generally used to favor the dispersion of cellulose, its content in the MFC was accounted for in the total composition when calculating the weight percentages of the formulations. Six different formulations were prepared following the composition indicated Table 1 (wt% refers to dry cellulose weight). Table S1 of the Supporting Information lists the measured weights of all components employed in the preparation of the composites. All the formulations were cross-linked in the oven for 3 h at 80 °C to study the influence of the cellulosic fillers on the curing process and on the final material.

2.4. Characterization

Fourier Transform Infra-Red (FTIR) analysis was performed in Attenuated Total Reflectance (ATR) mode with a Nicolet iS50 spectrometer (ThermoFisher Scientific Inc.) equipped with an ATR-Smart Orbit sampling accessory with a diamond crystal. The spectra were acquired in the 550–4000 cm^{-1} range, with 16 scans per spectrum and a resolution of 4 cm^{-1}. The conversion α of the cross-linking process was calculated from the average spectrum of 3 measurements for each sample by Eq. 2:

$$\alpha\,(\%) = \left(1 - \frac{A_t^{910}/A_t^{1580}}{A_{t_0}^{910}/A_{t_0}^{1580}}\right) \times 100 \qquad 2$$

where A_t^{910} is the area of the peak at 910 cm^{-1} (epoxy C—O) after 3 h, A_t^{1580} is the area of the peak at 1580 cm^{-1} (aromatic C═C), taken as internal reference, after 3 h, $A_{t_0}^{910}$ is the area of the peak at 910 cm^{-1} at initial time, $A_{t_0}^{1580}$ is the area of the peak at 1580 cm^{-1} at initial time.

Gel content (gel %) test in acetone was carried out to quantify the cross-linked fraction of polymer: samples of ca. 200 mg were cut in small pieces, weighted (m_0), wrapped in metallic nets and soaked for 24 h in 10 mL of acetone; they were then taken out from acetone and dried under fume hood for 24 h and finally in the oven at 100 °C for 2 h. The so-obtained masses (m_1) of the samples were used to calculate the gel % of the epoxy matrix by Eq. 3 after correction of the initial and final values considering the mass of the cellulose fibers, m_f.

$$gel\% = \frac{(m_1 - m_f)}{(m_0 - m_f)} \times 100 \qquad 3$$

Water absorption test was performed to check the swelling ratio (i.e., $swelling_{dry}$) of the cross-linked formulations. Samples of ca. 250 mg were soaked in 10 mL of ultrapure water. After 1 week they were taken out from water and gently wiped to remove the water from the surface; they were weighed (m_{1week}) and then dried in the oven at 100 °C for 6 h. Eventually, they were weighed again (m_0) and the swelling ratio was calculated by Eq. 4. For comparison, thus taking into account that glycerol is soluble in water, a second swelling ratio (i.e., $swelling_0$) was also calculated using m_0 measured before immersing the samples in water.

$$swelling\ ratio\% = \frac{m_{1week} - m_0}{m_0} \times 100 \qquad 4$$

Dynamic differential scanning calorimetry (DSC) was performed on 5–10 mg samples for each formulation with a Mettler Toledo Differential Scanning Calorimeter under a constant nitrogen flow rate (20 mL/min) with the following temperature cycle: 1) from −70 °C to 200 °C at 5 °C/min; 2) 200 °C for 2 min; 3) from 200 °C to −70 °C at 5 °C/min; 4) -70 °C for 2 min; 5) from −70 °C to 200 °C at 5 °C/min. Also, isothermal DSC with the same instrument was performed at 80 °C for 3 h for each formulation to check the absence of residual enthalpy after the curing cycle in the oven. Dynamic DSC from −30 °C to 180 °C at 10 °C/min was performed on cross-linked and reshaped formulations to check glass transitions and potential residual cross-linking too. Glass transition temperature T_g was determined by the transition onset point.

Thermogravimetric analysis (TGA) was performed with an ATG/DSC3+ from Mettler-Toledo in Al_2O_3 crucibles under nitrogen with a debit of 50 mL/min and a 10 °C/min ramp. TGA was performed on each formulation and on the samples before and after mechanical reshaping.

Dynamic Mechanical Analysis (DMA) tests were conducted on a TA Instruments DMA 850, from 25 °C to 180 °C at a rate of 3 °C/min. After applying a 0.05 N preload force, a constant deformation of 20 μm was chosen with a regular frequency of 1 Hz in tensile mode. The dimensions of the samples averaged 6 mm × 5 mm × 1.5 mm. DMA was performed on the samples before and after mechanical reshaping.

Stress relaxation experiments were performed for each cross-linked material to evaluate the rate of dynamic bond exchange with the Anton Paar Modular Compact Rheometer MCR 302 equipped with HPTD200 oven. The test was carried out using an 8 mm plate to plate geometry on 1.5–2.0 mm thick disks of the cross-linked polymer without fillers and with the highest amount of fillers (13MFC + 13UFC) at temperatures ranging from 140 °C to 180 °C. *C. prior* to the experiments a 1 % strain was applied with a constant normal force of 1 N for the samples without fillers and 5 N for the samples with fillers.

Rheological tests were performed to determine the viscoelastic properties of the formulations by using an Anton Paar Modular Compact Rheometer MCR 302 using a 25 mm plate to plate geometry. Amplitude sweep test at 1 Hz was performed to determine the viscoelastic parameters (G' and G") between shear strain (γ) = 0.01 and 100 % and to determine the yield stress (τ_0) at cross-point (ζ) between G' and G". Three interval Thixotropy Test (3iTT) was performed to simulate the printing process with the following three consecutive steps: 1) strain rate = 0.01 s^{-1} to have viscosity values almost at rest; 2) strain rate = 1 s^{-1} to have structural breakdown under high shear conditions; 3) strain rate = 0.01 s^{-1} to have structural regeneration almost at rest. Flow curves between 0.01 and 100 s^{-1} of shear rate were obtained for determining the viscosity trend with shear rate. Herschel-Bulkley model was applied on data from flow curves and yield stress from amplitude sweep test to determine the printability of the pastes.

Both the formulations NoFiller and 13MFC + 13UFC were successfully mechanically reshaped by using Carver Model C laboratory hot press at 160 °C under 3.5 metric tons for 1.5 h. The 3D printed piece made with the 13MFC + 13UFC formulation was reshaped as well using the same conditions.

2.5. 3D printing of the vitrimer paste by liquid deposition modeling

A Sidewinder SW-X2 Black (Artillery) FDM 3D printer was adapted for LDM by adding an extruder for clay produced by WASP fed by a pneumatic syringe. The system was used for 3D printing the composite paste with the highest concentration of fillers (13MFC + 13UFC). The software Simplify3D was used to set the printing parameters and the g-code files were exported and used for printing. An extruder nozzle of 1.0 mm was used with a resulting extrusion width of 1.1 mm. The printing was performed with the following parameters: infill = 0 % or 45 %, layer thickness = 0.9 mm and extruder movement speed = 500 mm/min.

To improve the curing cycle of the 13MFC + 13UFC formulation (after the printing process), the paste was placed on a parallel plate rheometer (25 mm diameter plate) and cured at 35 °C for 24 h and storage (G') and loss (G") modulus and viscosity were monitored by applying uniaxial stress of 1 % and a frequency of 1 rad/s.

2.6. Life cycle assessment (LCA)

This study is implemented as a deterministic screening LCA based on laboratory-scale measurements and single-parameter inventories. The objective is to provide preliminary environmental insights to orient material development at low Technology Readiness Level (TRL). The

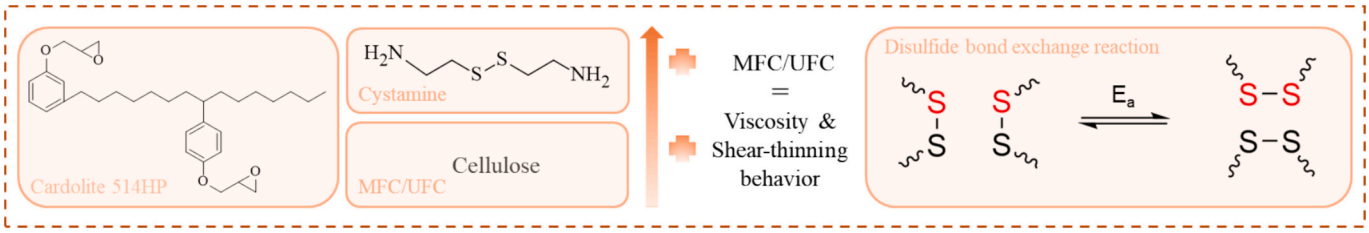

Fig. 1. Cardolite 514HP/cystamine vitrimer: schematic illustration of the dual reversible dynamic cross-linking network through dynamic disulfide bonds with the presence of MFC/UFC as rheology enhancers.

Life Cycle Inventory (LCI) was developed using primary data from laboratory experiments for all foreground processes. Background data for upstream processes were sourced from the Ecoinvent database (v3.11). The bio-based epoxy resin 514HP was modeled by adapting a standard fossil-based epoxy dataset, substituting bisphenol A with a bio-based cardanol derivative (NX-2026) based on its EPD data. A two-step process was modeled for cystamine preparation: 1) synthesis of cystamine dihydrochloride was reconstructed from patent CN109503441B [47]; 2) the desalination step was modeled using primary lab data, assuming 90 % solvent recovery. For the cellulosic fillers, as supplier LCI data was unavailable, the energy for mechanical milling was estimated using Von Rittinger's law [48]. Electricity for all lab operations was estimated from equipment specifications and operational durations. Full details on the LCI are documented in the supplementary spreadsheet. This screening-LCA is subject to some methodological limitations. The LCI for key precursors like cystamine carries inherent uncertainty due to its reconstruction from patent literature, and the energy models are based on lab-scale equipment not representative of industrial efficiencies. Furthermore, the assessment scope was limited to seven impact categories, omitting others relevant for bio-based systems like land use and water scarcity. The primary analysis also assumes an idealized 100 % material recovery in reshaping scenarios; however, the robustness of this and other key assumptions is directly tested in the sensitivity analysis.

Eventually, as mechanical performance data are still evolving, a mass-based functional unit (1 kg of vitrimer formulation) was selected. However, being the present LCA subjected to several sources of uncertainty, including the use of laboratory-scale energy data, proxy datasets, and simplified stoichiometric inventories, the reported impacts should be interpreted as indicative trends rather than precise predictions.

3. Results and discussion

In pursuit of more sustainable materials for eco-friendly epoxy systems in 3D printing, herein a bio-based vitrimer was developed using an epoxy resin derived from cardanol (514HP) and cross-linked with cystamine (Fig. 1). Cystamine was chosen for its renewable origin, reactive aliphatic amine groups, which promote efficient network formation under relatively low thermal conditions, and dynamic disulfide linkages. These unique bonds are capable of undergoing disulfide exchange reactions (Fig. 1), which can be exploited to enable the mechanical reprocessing of the vitrimer network.

To create printable pastes suitable for LDM 3D printing, MFC and UFC were introduced as natural fillers and rheological modifiers. In particular, six different vitrimer formulations were prepared increasing the amount of dry cellulose (see Table 1). MFC and UFC were used both separately and together, with a content up to 13 dry wt% of both fillers. The epoxy-amine formulation without filler (NoFiller) was used as reference.

3.1. Curing and characterization of the cured vitrimers

The reactivity of the six formulations was first studied via isothermal DSC at 80 °C. This curing temperature was selected to prevent the thermal degradation of cystamine, which is sensitive to elevated temperatures (> 180 °C) when not cross-linked. This choice is supported by the TGA of desalinated cystamine, presented in Fig. S3 of the Supporting Information alongside the TGA curve of the 514HP resin, confirming the stability of cystamine under the selected curing conditions. Furthermore, curing at low temperatures helps avoid bubbles formation caused by the evaporation of water from the cellulosic fillers. The corresponding isothermal DSC curves are shown in Fig. S4 of the Supporting Information. A general decrease in the reaction rate was observed upon the addition of fillers, especially with MFC. This effect was attributed to the presence of both water and glycerol, which diluted the reacting mixture and promoted competitive opening of the epoxy groups. The influence of glycerol on the reaction was confirmed by heating a mixture of glycerol and 514HP resin at 80 °C for 3 h; FTIR-ATR analysis before and after heating revealed a slight decrease in the epoxy ring signal at 910 cm^{-1}, accompanied by a strong reduction in the O—H stretching band at 3200–3400 cm^{-1} (Fig. S5 of the Supporting Information). Conversely, no change in reaction rate was observed when higher concentrations of UFC were added to the 13MFC formulation, indicating that UFC alone does not significantly affect the curing kinetics. Overall, no residual enthalpy was detected after three hours of curing. For this reason, all subsequent cross-linking procedures were conducted at 80 °C for 3 h after pouring the formulations into silicone molds. Notably, the cardanol-based system investigated in this study achieved complete cross-linking at a lower temperature than other cardanol-based systems reported in the literature [11,20,49], demonstrating improved energy efficiency.

The cross-linking was verified by FTIR analyses performed in ATR mode before and after curing (Fig. S6 of the Supporting Information). The reaction was monitored by the disappearance of oxirane signals at 826 cm^{-1}, 910 cm^{-1} and 3000 cm^{-1}, accompanied by a concurrent increase of the O—H group stretching signal at 3200–3400 cm^{-1} [50,51]. Conversion (α) of the epoxy groups was calculated as described in the Experimental Section, and the resulting values are shown in Table *1*. While complete consumption of epoxy groups was observed for the sample without fillers (no residual peak at 910 cm^{-1}), when cellulosic fillers were used, a general decrease of conversion was noticed, with a minimum of 92 % for the 13MFC + 11UFC sample. Furthermore, the 13MFC sample exhibited a gradient in conversion across its thickness: values of 83 % in the upper part (in contact with air during curing) and of 95 % in the bottom part (on the base of the mold) were obtained. This is because, at high temperatures, glycerol tends to separate from the MFC and accumulate on the surface of the sample, diluting the reactive mixture and causing a conversion gradient throughout the thickness of the cross-linked material (see Fig. S7 in the Supporting Information). However, when MFC was used in combination with UFC, no gradient in conversion values was noticed, indicating that UFC effectively suppressed the upward migration of glycerol, resulting in more homogeneous samples. The inhibition of additive migration, such as plasticizers or dyes, by cellulose has been previously documented in the literature, supporting this hypothesis [52,53]. To further validate these findings, dynamic DSC analyses were performed on each formulation immediately after mixing using crude samples: the corresponding DSC curves

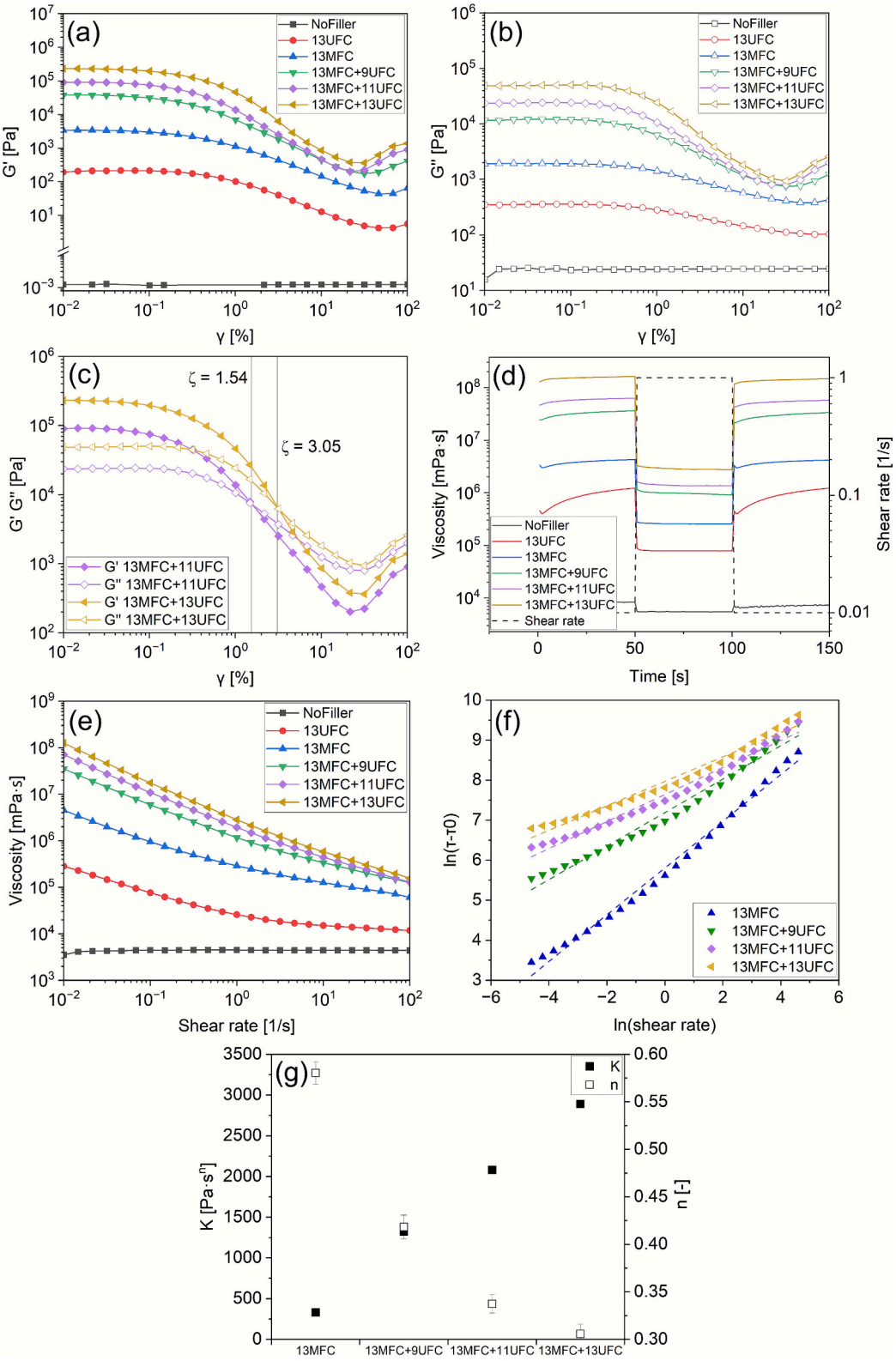

Fig. 2. Rheological analyses of the pastes: amplitude sweep test results of storage modulus G' (a) and loss modulus G" (b) of each formulation; cross-point ζ of 13MFC + 11UFC and 13MFC + 13UFC formulations (c); 3iTT chart (d), and flow curves of each formulation (e); Herschel-Bulkley fitting (f) and flow consistency index K and flow behavior index n with corresponding error bars (g) for selected formulations with a yield stress.

are shown in Fig. S8 of the Supporting Information. Values of glass transition temperature T_g (taken at onset) before ($T_{g\text{-}pre}$) and after ($T_{g\text{-}post}$) cross-linking, cross-linking enthalpy (ΔH_c) after correction considering the cellulose fraction, reaction temperature onset (T_{onset}) and peak (T_{peak}) are listed in Table S2 of the Supporting Information. When fillers were added, an increase in T_{onset} and T_{peak} was observed, confirming a decrease in the cross-linking rate. Simultaneously, a decrease in reaction enthalpy (−13 % ca. for 13UFC sample and − 21 %

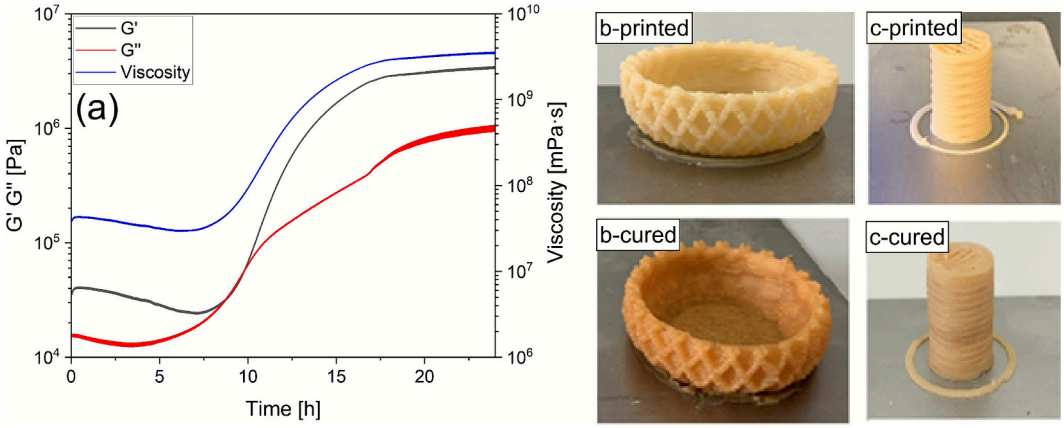

Fig. 3. Printing by LDM: storage modulus (G'), loss modulus (G") and viscosity vs time at 35 °C for the 13MFC + 13UFC formulation (a); printed vase (b) and filled cylinder (c) before and after curing in the oven.

ca. for the samples with MFC) was noticed, also confirming the reduction of cross-linking degree when cellulosic fillers were used.

To further confirm the efficiency of the curing reaction, the insoluble fraction and the water swelling behavior of the cross-linked materials were evaluated, and the results are reported in Table *1*. Compared to the unfilled system, a decrease in gel content values was observed when MFC was used, with a minimum of 80.8 % for the 13MFC sample. This decrease can be ascribed both to the dissolution of glycerol during the extraction test and to its influence on the cross-linking degree, which likely contributes to a lower network density. This influence was also confirmed by the swelling test ($swelling_{dry}$) in water: while a negligible swelling value was observed for the sample without fillers, the introduction of MFC strongly increased the water uptake, due to the hydrophilicity of MFC itself and the decrease of cross-linking density. The addition of UFC did not modify the insoluble fraction, and adding UFC to the formulations with MFC even caused a slight increase in gel content values compared to the sample with only MFC. Moreover, the inclusion of UFC caused only a slight increase in $swelling_{dry}$, due to the presence of ultrafine cellulose between the cross-linking bonds. The highest swelling value was observed for the 13MFC + 11UFC formulation ($swelling_{dry}$ = 29.5 ± 0.3 %), due to the combined effects of the larger particle size of MFC and the reduction of cross-linking density caused by side reactions involving glycerol. Overall, the swelling behavior of the composite vitrimers arises from the interplay among glycerol dissolution during the test, the hydrophilicity of the cellulose fillers, and the structure of the cross-linked network. However, as demonstrated by the comparison with $swelling_0$ values, which are significantly lower than the previously reported values of $swelling_{dry}$, the dissolution of glycerol in water has a pronounced effect. When m_0 was measured prior to immersion, the maximum actual swelling was 13.9 % for the 13MFC + 13UFC sample.

Dynamic DSC analyses were also performed on cured samples (in oven) and the measured T_g values are listed in Table *1*: the results show only a slight decrease in glass transition temperature with the addition of cellulose, attributed to the lower epoxy conversion (Fig. S9 of the Supporting Information).

The cross-linked samples were also characterized by TGA, to evaluate their thermal resistance and to confirm the composition. The thermograms are displayed in Fig. S10 of the Supporting Information. Generally, the samples exhibited good thermal stability, with a decrease in $T_{5\%}$ values (i.e., the temperature at 5 % of weight loss, Table 1) for the sample containing MFC, due to the presence of glycerol. The degradation of glycerol was confirmed by TGA of MFC and by literature as well [45,46]. Two other degradation steps can be observed, the first starting at 250 °C and the second one at 310 °C, mainly attributed respectively to the cystamine fraction and to the 514HP fraction. Eventually, as expected, the residual char at the end of the analysis increased at higher cellulose content.

3.2. Rheology characterization of the pastes

In order to select the most appropriate paste for printing, each of the six formulations was characterized by rheological measurements. An amplitude sweep test was performed to evaluate the storage (G') and loss (G") moduli. Information about yield stress (τ_0), which is fundamental for 3D printing evaluation, was also obtained. The results are presented in Fig. 2a-c. An increase in modulus values was observed with a higher filler content. A higher increase was observed when MFC was used instead of UFC (see results for 13MFC and 13UFC), however using higher amounts of MFC was not possible due to issues inherent to the presence of water and glycerol as previously discussed. For NoFiller and 13UFC samples, a G" higher than G' throughout the entire shear strain interval was observed, meaning that they behave as liquid regardless of the applied shear strain. However, all other formulations presented a G' higher than G" at low shear strain and a cross-point ζ where G" became higher than G'. This indicates that they have solid-like behavior at low shear rates and liquid-like behavior at high shear rates, typical of shear-thinning fluids. Furthermore, the cross-point ζ shifted to higher shear strain by increasing the filler content. This behavior is necessary for LDM printing, but it is not sufficient on its own to define the paste as 3D printable. The modulus of the paste must be high enough to prevent the collapse of the 3D printed structures due to atmospheric pressure.

A Three interval Thixotropy Test (3iTT) test in the shear rate range of 0.01 to 1 s^{-1} was performed to study the thixotropy of the pastes (see Fig. 2d). The variation in shear rate is representative of the three steps of the printing process: 1) material at rest in the syringe (low shear rate); 2) material flowing through the extruder (high shear rate); 3) extruded material deposited on the printing plate (low shear rate). Despite a certain degree of thixotropy can be useful for 3D printing, a paste with low thixotropy (i.e., stable viscosity trend following shear rate changes) is also preferred over a material with too high thixotropy. In fact, once extruded, the material must stop flowing as quickly as possible to maintain its shape and avoid following the movement of the extruder. In general, pastes containing MFC showed better thixotropy behavior than those formulated with only UFC, confirming the importance of including MFC in the formulations. Furthermore, a greater difference in viscosity between low and high shear rates can enhance paste printability. Flow curve tests between 0.01 and 100 s^{-1} were performed to obtain the dependence of viscosity on the shear rate. The results are shown in Fig. 2e. The addition of the cellulosic fillers produces a shear-thinning material (i.e., viscosity decreases with an increasing shear rate). As expected and confirmed by 3iTT and amplitude sweep tests, MFC has a higher impact on viscosity than UFC. In fact, at low shear rates the

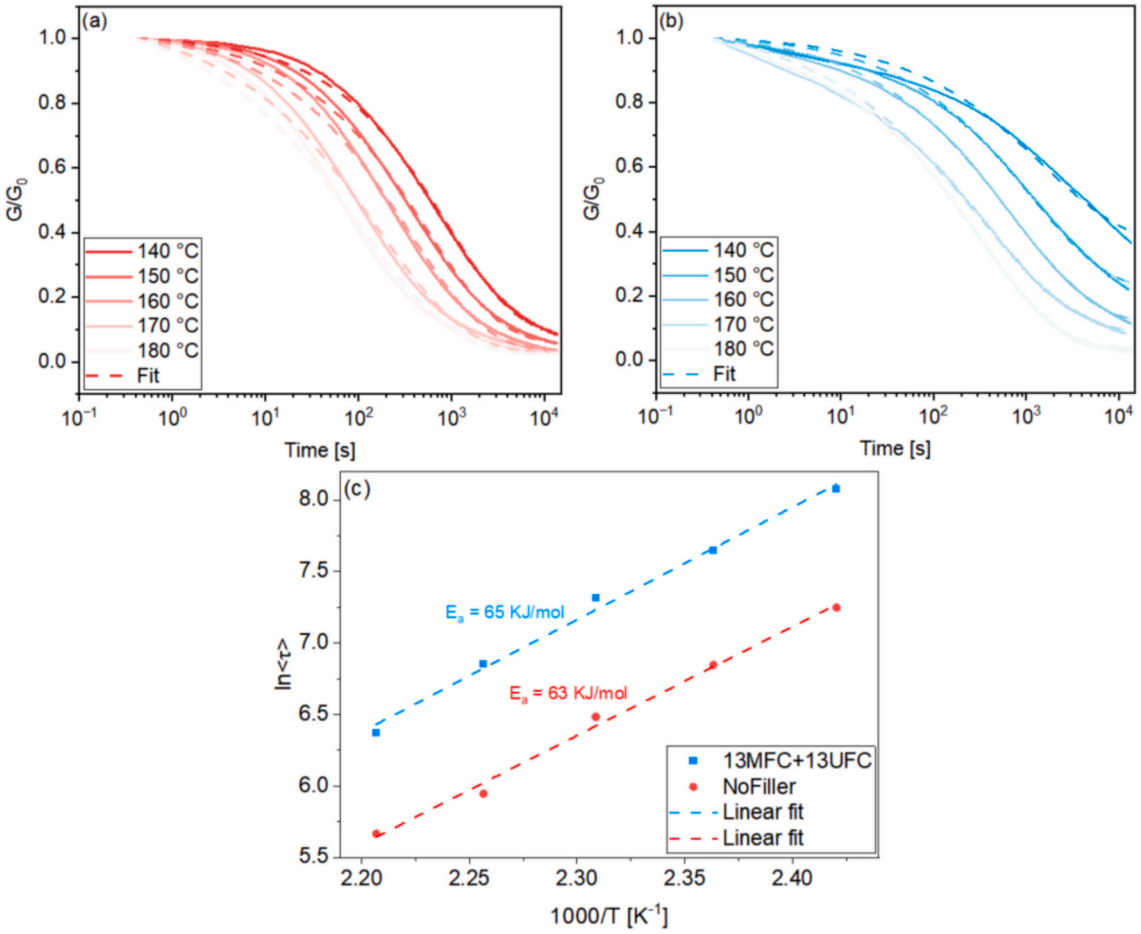

Fig. 4. Modified KWW fitted normalized stress relaxation measurements for samples NoFiller (a) and 13MFC + 13UFC (b); characteristic average relaxation time $< \tau >$ vs 1000/T for samples NoFiller (red) and 13MFC + 13UFC (blue) (c).

13MFC paste has a viscosity value 1000 times higher than the one of 13UFC. By adding UFC to MFC, a gradual increase of viscosity can be noticed, with a more marked difference at low shear rate. The magnitude of the viscosity drop at high shear rates is important, as it indicates pronounced shear-thinning behavior and good flow during extrusion.

The values of shear stress obtained from the flow curves were fitted to the Herschel-Bulkley model (Eq. 5) using τ_0 as the yield stress obtained from amplitude sweep measurements [54,55]:

$$ln(\tau - \tau 0) = lnK + nln(shear\ rate) \quad 5$$

where τ is the applied shear stress obtained from flow curves measurements, τ_0 is the yield stress, K is the flow consistency index and n is the flow behavior index. For printing by LDM, a low value of n and a high value of K are desirable: this is usually associated with a better shape-preservation and an enhanced shear-thinning behavior. Furthermore, a high τ_0 is usually associated with higher moduli, which are needed to prevent the collapse of the printed structure and to enable the layers to efficiently support the weight of the upper layers. The fitting results are depicted in Fig. 2f-g. As expected, by increasing the fillers amount, the n values decrease to a minimum of 0.31 and the K values increase to a maximum of 2890 Pa·s^n for the 13MFC + 13UFC formulation, indicating higher yield stress and shear thinning behavior. Based on the results from rheology tests, the 13MFC + 13UFC paste was selected for 3D printing.

3.3. 3D printing by liquid deposition modeling

3D printing was performed on the 13MFC + 13UFC formulation by LDM. To prevent the collapse of the 3D printed structure during the curing step in the oven, a rheological plate-to-plate isothermal test at 35 °C was performed to monitor the evolution of G', G" and viscosity versus time. A uniaxial stress of 1 % and a frequency of 1 rad/s were applied. The results, shown in Fig. 3a, indicate that although the printed paste immediately retains its geometry due to its rheology-driven solidity, chemical gelation at 35 °C proceeds gradually. An increase in G' and G" was observed after approximately 9 and 6 h, respectively, and the gelation time (t_{gel}), identified as the point of maximum viscosity increase, occurred between 10 and 12.5 h. After this point the temperature can be increased, while preserving the shape.

For this reason, the curing cycle consisted of an initial step at 35 °C for 12 h to stabilize the printed structure, followed by a second step at 80 °C for 3 h to achieve complete conversion and optimal thermo-mechanical properties. Two different shapes were printed (Fig. 3b-c): a vase without infill and a cylinder with 45 % infill, both with same printing parameters. The fidelity index (F_i) for the cylinder shape, which reflects the printing precision measuring how accurately the shape of the printed object matches its original digital design (CAD model), was calculated by Eq. 6:

$$fidelity\ index\ (\%) = \frac{S_{Pr}}{S_{Th}} \times 100 \quad 6$$

where S_{Pr} is the vertical section of the printed cylinder and S_{Th} is the vertical section of the theoretical cylinder. A F_i value equal to 87.0 % was obtained, indicating good fidelity. No difference in size of the shape was observed before and after curing.

Table 2
Values of τ*, β and $<\tau>$ at each analyzed temperature for NoFiller and 13MFC + 13UFC formulations.

	NoFiller				13MFC + 13UFC			
T [°C]	β [−]	τ* [s]	$<\tau>$ [s]	R^2	β [−]	τ* [s]	$<\tau>$ [s]	R^2
140	0.58	896	1406	0.999	0.49	1575	3227	0.988
150	0.54	536	942	0.998	0.52	1114	2089	0.998
160	0.52	353	654	0.997	0.48	708	1505	0.999
170	0.46	163	382	0.994	0.41	314	947	0.999
180	0.43	105	289	0.989	0.47	263	584	0.999

3.4. Stress relaxation and reprocessing of the cured vitrimers

The dynamic bond exchange rate of the vitrimers without fillers and with the highest amount of cellulose (13MFC + 13UFC, which has been used for LDM) was analyzed by stress relaxation measurements. A constant strain of 1 % was applied at five different temperatures ranging from 140 °C to 180 °C (the upper limit determined by TGA measurements) and the normalized relaxation modulus G/G_0 was monitored as a function of time. The relaxation curves were fitted to the Kohlrausch−Williams−Watts (KWW) stretched exponential decay reported in Eq. 7, modified taking into account that the relaxation modulus was normalized to the initial value taken at 0.4 s [56–58].

$$G(t)\Big/G_0 = G_{res}\Big/G_0 + (1 - G_{res}/G_0)\exp\left[(0.4/\tau^*)^{\beta} - (t/\tau^*)^{\beta}\right] \quad 7$$

where $G(t)/G_0$ is the normalized stress at time t, G_{res}/G_0 is the fraction of residual relaxation modulus, τ* is the characteristic relaxation time and β ($0 < \beta \leq 1$) is the stretching exponent that controls the shape of the stretched exponential decay and reflects the breadth of the relaxation distribution. The smaller the value of β, the broader the distribution of relaxation times. The characteristic average relaxation time $<\tau>$ of the stretched exponential decay was subsequently calculated by Eq. 8.

$$<\tau> = (\tau^*\Gamma(1/\beta))/\beta \quad 8$$

where Γ is the mathematical gamma function [59]. The KWW normalized fitted curves are shown in Fig. 4a-b. Values of β, τ* and $<\tau>$ are listed in Table 2. A general increase in the characteristic average relaxation time was observed for the 13MFC + 13UFC samples compared to those without cellulose. The presence of cellulose slowed down the relaxation of the vitrimer that still had complete relaxation at $T \geq 170$ °C, but incomplete relaxation at lower temperatures (at 140 °C: $G_{res}/G_0 = 0.36$; at 150 °C: $G_{res}/G_0 = 0.22$; at 160 °C: $G_{res}/G_0 = 0.11$). Furthermore, overall lower values of β were observed for the 13MFC + 13UFC samples, suggesting a wider distribution of relaxation dynamics. In general, when no filler was used, the values of β were comparable to the ones found for other vitrimers based on cystamine [21]. When considering relaxation times, our NoFiller system exhibited values approximately one order of magnitude higher than those reported in the literature for a similar system combining cystamine with a vanillin-based epoxy. For instance, Guggari et al. reported relaxation times of 73.7 s and 22.1 s at 140 °C and 170 °C, respectively [21]. However, when comparing our cardanol-based system with another system based on transesterification reactions, lower relaxation times were observed overall. Hu et al. reported relaxation times of 48.2 min at 140 °C and 6.2 min at 200 °C, which are considerably higher than those obtained for our vitrimer system [20]. These findings demonstrate that the incorporation of disulfide bonds in the crosslinker significantly enhances the dynamic behavior and reprocessability of the developed cardanol-based vitrimer.

Values of activation energy (E_a) were calculated by fitting the relationship between $\ln<\tau>$ vs 1000/T to the Arrhenius equation for both formulations. The fitted curves are showed in Fig. 4c. Values of 63 kJ mol^{-1} and 65 kJ mol^{-1} with a R^2 value of 0.99 were obtained for NoFiller and 13MFC + 13UFC formulations, respectively. These values are comparable to those previously published for formulations based on cystamine; however, activation energies are known to depend strongly on various materials' parameters [60]. Notably, the incorporation of fillers does not significantly affect E_a, but only slightly slows down the exchange kinetics, likely due to restricted molecular mobility. This result thus demonstrates that the introduction of fillers can enhance the functionality of the vitrimer network without compromising its dynamic characteristics.

Samples without (NoFiller) and with the highest concentration of fillers (13MFC + 13UFC) were then cut in half and hot-pressed in a 15 mm × 25 mm rectangular closed geometry mold. The process was carried out at 160 °C and was repeated two times to demonstrate reshapability. The resulted samples were analyzed by FTIR-ATR (Fig. 5a), TGA

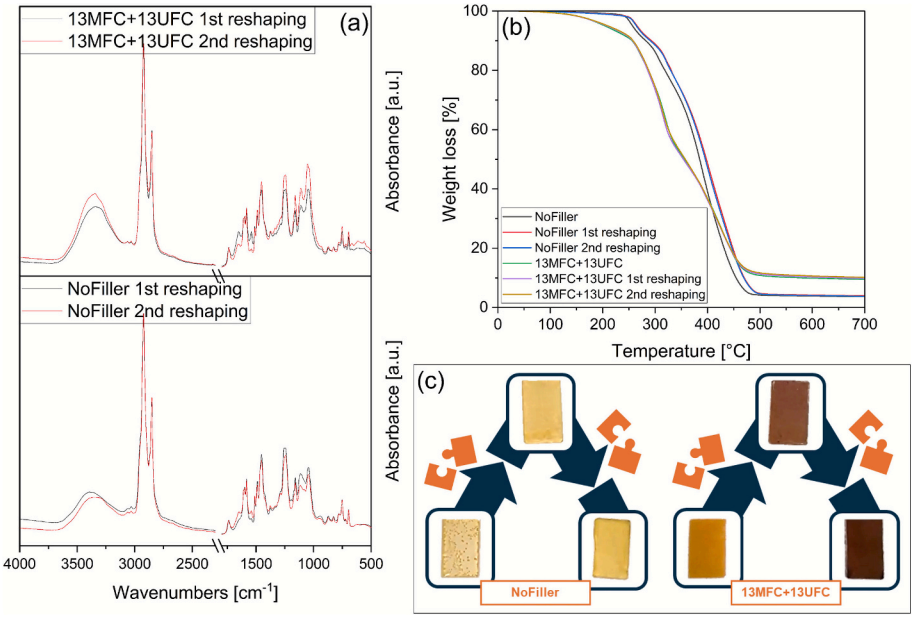

Fig. 5. Reshaping of vitrimers: FTIR-ATR spectra (a) and TGA curves (b) of samples after the 1st and 2nd reshaping steps with the corresponding pictures (c).

Table 3
Values of conversion (α), gel content (gel %), swelling$_0$ and $T_{5\%}$ of samples after the 1st and 2nd reshaping steps.

	1st reshaping step				2nd reshaping step			
	α [%]	Gel content [%]	Swelling$_0$ [%]	$T_{5\%}$ [°C]	α [%]	Gel content [%]	Swelling$_0$ [%]	$T_{5\%}$ [°C]
NoFiller	100	99.7 ± 0.3	0.8 ± 0.1	265	100	99.3 ± 0.0	0.9 ± 0.1	264
13MFC + 13UFC	100	83.0 ± 1.2	13.0 ± 1.2	204	100	83.4 ± 2.1	14.1 ± 0.5	204

Table 4
Description of the various considered LCA scenarios, including manufacturing routes, material compositions, and key hypotheses (each scenario contemplates incineration as EoL treatment).

Scenario	Manufacturing	Filler	Mechanical reshaping	Number of uses	Key Hypotheses
C-NF	Casting	No	No	1	Virgin matrix, no filler, processed by casting, no reshaping
C-F	Casting	Yes	No	1	Matrix with filler, processed by casting, no reshaping
C-F + R	Casting	Yes	Yes (up to 2×)	3	Matrix with filler, processed by casting, closed-loop, full material recovery for up to 2 reshaping steps, properties maintained per experimental data (no significant degradation/ mass loss)
P-F	3D printing	Yes	No	1	Matrix with filler, 3D printed, no reshaping
P-F + R	3D printing	Yes	Yes (up to 2×)	3	Matrix with filler, 3D printed, closed-loop: same as C-F + R, but fabricated via 3D printing

(Fig. 5b), dynamic DSC and DMA (Fig. S11 and Fig. S12 of the Supporting Information, respectively). Fig. 5 depicts also the images of the samples before and after hot-pressing. The values of conversion (α), gel content, swelling$_0$ and $T_{5\%}$ of the samples after each reprocessing step are listed in Table 3. Images of bigger samples (70 mm × 40 mm) are also reported in Fig. S13 of the Supporting Information. While almost no change was observed for gel content and swelling values before and after reprocessing, confirming no change of soluble fraction and cross-linking density, a slight increase in conversion of epoxy groups was noticed. This small increase can be attributed to oxidation at high temperature of residual epoxy groups that did not previously react with the amine groups of cystamine during the cross-linking step in the oven at 80 °C. This interpretation is supported by the FTIR-ATR spectra, which show the appearance of a carboxylic signal at 1700 cm^{-1}. Furthermore, the samples became darker after hot pressing (Fig. 5c), particularly in the case of the filled system, a behavior commonly observed in epoxy thermosets as a result of oxidative phenomena [61]. The absence of air bubbles or residual crack confirmed the successful reshaping process and efficient flow of the vitrimer during the hot-pressing. Dynamic DSC measurements performed on the samples after each reshaping step showed no residual reaction enthalpy and no significant changes for both NoFiller and 13MFC + 13UFC samples. TGA analysis also confirmed the thermal stability of the materials after reshaping, with negligible variations observed. A slight improvement in thermal resistance was noted for the reshaped NoFiller samples, which exhibited a marginally higher $T_{5\%}$. Overall, the DMA results revealed negligible variations in the T_g values (approximately 55 °C) and comparable moduli across all reshaping cycles. The higher T_g values obtained from DSC (Table 1), relative to those from DMA, can be ascribed to the distinct physical phenomena probed by the two techniques and to differences in the applied heating rates. All these results demonstrate the successful feasibility of mechanically repairing and reshaping of the studied vitrimers, both with and without cellulosic fillers.

3.5. Life cycle assessment results of the vitrimer system

The primary objective of the Life Cycle Assessment (LCA) was to evaluate the environmental performance of the studied epoxy vitrimer system, focusing on the effects of matrix composition, fabrication method and End-of-Life (EoL) treatment. The LCA compared formulations with and without the cellulosic fillers, produced by either casting or 3D printing, across multiple EoL strategies. The results were intended to identify environmental hotspots and inform material selection and process optimization. The functional unit (FU) was defined as 250 g of vitrimer material: this corresponds to a batch size used in experiments including ≈ 50 individual samples (≈ 5 g each) for 3D printing and a single block of equivalent mass for casting. A cradle-to-grave system boundary was adopted, covering raw material extraction, formulation, fabrication, thermal curing, optional mechanical reshaping, and final EoL treatment (Fig. S14 of the Supporting Information). The use phase was considered environmentally neutral. Five scenarios were defined, as summarized in Table 4. In reshaping scenarios (C-F + R, P-F + R), initial production impacts are allocated equally across three use cycles. The additional energy for each reshaping operation is added to the respective cycle.

The aggregated results for each scenario are presented in Fig. 6. Across all scenarios, the upstream synthesis of desalinized cystamine was unequivocally identified as the dominant environmental hotspot, contributing to the majority of impacts for Global Warming Potential (GWP), fossil fuel depletion and toxicity potentials. The introduction of the cellulosic fillers improves the environmental profile by displacing a fraction of the high-impact epoxy-cystamine matrix. In particular, screening-level results indicate a potential reduction in GWP for formulations incorporating cellulose fillers, mainly due to lower epoxy content and the reduced impacts of bio-based components. Such a result is particularly noteworthy given that the addition of cellulose fillers is essential for enabling 3D printing; thus, they not only facilitate the processing of the material but also enhance its overall sustainability. Comparing C-F + R and C—F scenarios, it can be noticed that the advantage of reusability is significant. Allocating the initial production impacts over three uses reduces the per-use GWP of the reshaped vitrimer (C-F + R) by 36 % compared to its single-use counterpart. The recurring energy for hot-pressing is minor in comparison to the

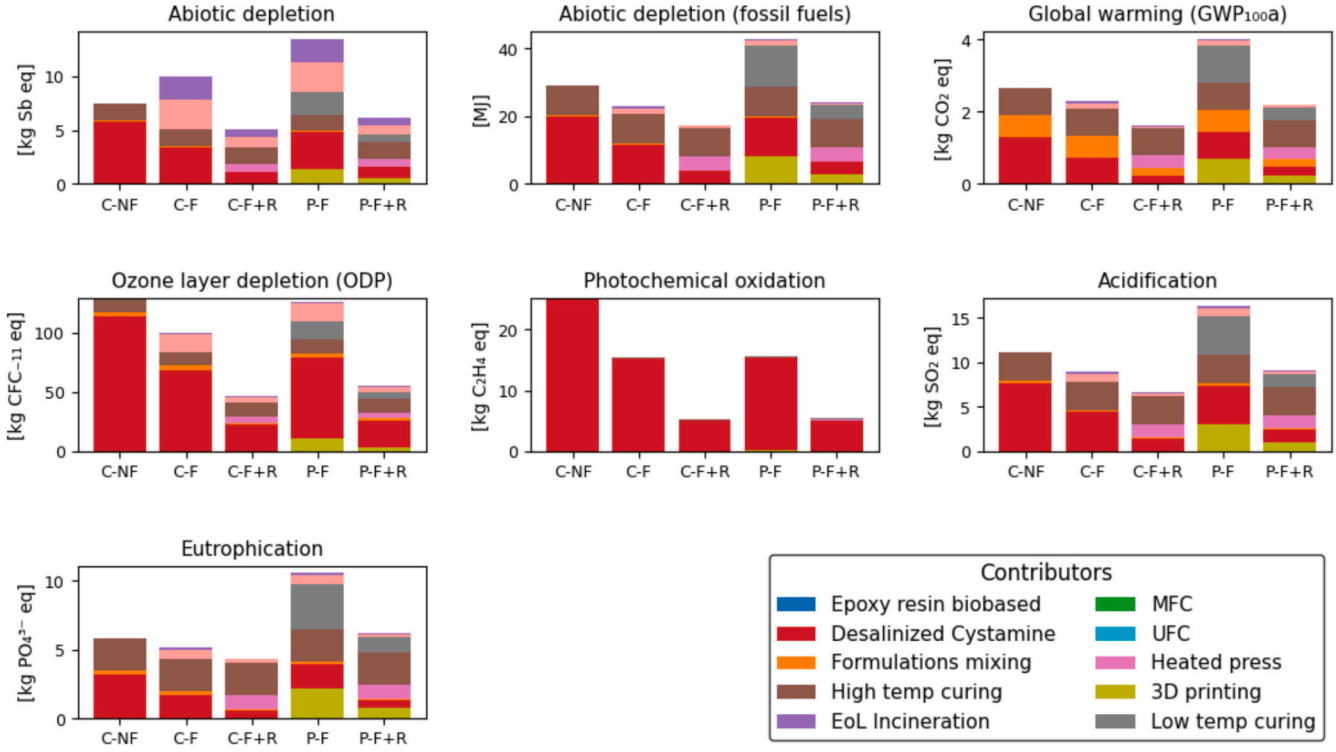

Fig. 6. LCA results: stacked contribution analysis for each scenario.

"amortized" impact of material production. From comparison of P—F and C—F scenarios, the 3D printing process (P—F) exhibits a higher impact than cast molding (C—F), with a 63 % higher GWP. This is attributed to the process-level inefficiencies of fabricating numerous small, discrete parts versus a single bulk object, which leads to higher cumulative energy consumption. Nonetheless, 3D printing provides significant advantages in terms of design flexibility, material efficiency, and the capability to produce complex, customized polymer structures. Therefore, the selection of the processing technique should not be based solely on environmental impact, but must also consider the specific requirements of the intended application. It is critical to note that once the 3D printed part is reshaped, it can no longer be reprinted. While the material is mechanically reshapable, its unique additive manufacturing capability is lost, representing a form of functional downcycling.

As the LCA results are based on laboratory-scale data, they should be interpreted as indicative trends. To evaluate the robustness of the study's conclusions against key modeling assumptions, a sensitivity analysis was performed on the GWP results for all relevant scenarios. The GWP contribution from the cystamine LCI, the primary environmental hotspot, was varied by ±50 % to account for data uncertainty. The results (Fig. S15a of the Supporting Information) show that while the absolute GWP scores fluctuate, the relative ranking of the scenarios is unequivocally preserved for both manufacturing methods. The reshaped cast-molded vitrimer (C-F + R) consistently shows a significantly lower GWP than its single-use counterpart (C—F) across the entire uncertainty range. The same holds true for the 3D printed scenarios (P-F + R vs. P—F). This confirms that the conclusion that reshaping is environmentally preferable is highly robust against uncertainty in the main impact driver. Furthermore, the reshaping scenarios were re-modeled to assess the impact of non-ideal material recovery, testing 100 % (ideal), 95 %, and a conservative 90 % recovery rate per cycle, with losses replenished by virgin material (Fig. S15b of the Supporting Information). The analysis shows that even in the most conservative case of 90 % recovery, the environmental benefit of reshaping remains substantial. The per-use GWP of the reshaped casted vitrimer (C-F + R) is 33 % lower than its single-use version. This advantage is even more pronounced for the 3D printed scenario (P-F + R), which maintains a GWP over 45 % lower than its single-use benchmark. This analysis confirms that the study's primary findings, namely that reshaping provides a strong environmental benefit regardless of manufacturing method, and that cast molding is more efficient at this scale, are robust and not artifacts of idealized modeling assumptions. Overall, the LCA demonstrates that reshaping markedly lowers per-use environmental impacts, underscoring the relevance of this fully bio-based vitrimer in the context of sustainable additive manufacturing.

4. Conclusions

In this work, a fully biobased epoxy vitrimer based on disulfide bond exchange was successfully formulated and processed by LDM 3D printing, employing ultrafine cellulose and microfibrillated cellulose as rheology modifiers. Cystamine was used as cross-linker, enabling curing of printed structures at temperatures low enough to prevent deformation in the oven, yet high enough to avoid premature cross-linking during printing. Systems with and without cellulosic fillers were fully characterized, and the curing cycle was optimized by DSC, gel content and swelling measurements. Rheological tests identified 13 wt% MFC and 13 wt% UFC as optimal filler concentrations for balancing shear-flow behavior and post-print structural integrity. The pastes were successfully printed in various shapes and cured through a two-step low temperature process (12 h at 35 °C and 3 h at 80 °C), achieving a final shape fidelity index of 87.0 %. The vitrimer behavior of the materials was confirmed for both filled and unfilled systems by stress-relaxation tests, which revealed fast relaxation times (654 s and 1505 s at 160 °C for unfilled and filled systems, respectively). Mechanical reshaping by hot pressing (1.5 h at 160 °C, 3.5 metric tons) demonstrated full recyclability, with DSC, TGA, DMA and gel content analyses showing no degradation in performance after repeated cycles. The preliminary LCA provided comparative insights into the environmental performance of the vitrimer systems. Screening-level results suggested a potential reduction in GWP for cellulose-filled systems, driven by the partial substitution of epoxy resin with low-impact fillers, confirming the dual

role in enabling LDM printing and improving sustainability. Moreover, compared to a single-use lifecycle, reprocessing reduced the GWP by 36 % for cast-molded and up to 48 % for 3D-printed systems. Sensitivity analysis confirmed the robustness of the comparative conclusions, showing consistent scenario rankings under varying assumptions. The synthesis of the cystamine crosslinker was identified as the dominant environmental hotspot, underscoring the need for higher-quality, industrial-scale data to refine the environmental profile of the entire system. The novelty of this work lies in integrating a fully biobased vitrimer, capable of low temperature stabilization and reprocessability, into a formulation suitable for LDM, an approach not previously demonstrated for cardanol-based systems. The resulting materials are well suited for non-load-bearing applications such as flexible fixtures, housings, cushioning or damping elements, and customized geometries where print fidelity, sustainability, and recyclability are key requirements.

CRediT authorship contribution statement

Edoardo Albertini: Writing – review & editing, Writing – original draft, Visualization, Methodology, Investigation, Formal analysis, Conceptualization. **Mirko Busto:** Writing – original draft, Visualization, Methodology, Investigation, Formal analysis. **Sara Dalle Vacche:** Writing – review & editing, Investigation. **Gian Andrea Blengini:** Supervision, Resources, Funding acquisition. **Marc Guerre:** Writing – review & editing, Supervision, Resources, Methodology, Conceptualization. **Alessandra Vitale:** Writing – review & editing, Supervision, Resources, Funding acquisition, Conceptualization.

Declaration of competing interest

The authors declare that they have no known competing financial interests or personal relationships that could have appeared to influence the work reported in this paper.

Acknowledgments

This study was carried out within the MICS (Made in Italy—Circular and Sustainable) Extended Partnership and received funding from the European Union Next-Generation EU (PIANO NAZIONALE DI RIPRESA E RESILIENZA (PNRR) – MISSIONE 4 COMPONENTE 2, INVESTIMENTO 1.3 – D.D. 1551.11-10-2022, PE00000004). This manuscript reflects only the authors' views and opinions, and neither the European Union nor the European Commission can be considered responsible for them.

Appendix A. Supplementary data

Supplementary data to this article can be found online at https://doi.org/10.1016/j.cej.2025.172399.

Data availability

Data will be made available on request.

References

[1] F. Bezzi, P. Fabbri, G. Magnani, E. Salernitano, M. Scafè, A. Strafella, Aqueous aluminium titanate paste for the liquid deposition modelling, Open Ceramics 9 (2022) 100224, https://doi.org/10.1016/j.oceram.2022.100224.
[2] B. Gyawali, R. Haghnazar, P. Akula, K. Alba, V. Nasir, A review on 3D printing with clay and sawdust/natural fibers: printability, rheology, properties, and applications, Results Eng. 24 (2024) 103024, https://doi.org/10.1016/j.rineng.2024.103024.
[3] K. Bouzidi, Formulation of a Thermosetting Biocomposite Based on Poly (Furfuryl Alcohol) and Cellulose for 3D Printing, Université Grenoble Alpes [2020-..], 2022. https://theses.hal.science/tel-03983527.
[4] J.A. Lewis, Direct ink writing of 3D functional materials, Adv. Funct. Mater. 16 (2006) 2193–2204, https://doi.org/10.1002/adfm.200600434.
[5] H. Lopez Hernandez, J.W. Souza, E.A. Appel, A quantitative description for designing the Extrudability of shear-thinning physical hydrogels, Macromol. Biosci. 21 (2021) 2000295, https://doi.org/10.1002/mabi.202000295.
[6] G. Postiglione, G. Natale, G. Griffini, M. Levi, S. Turri, Conductive 3D microstructures by direct 3D printing of polymer/carbon nanotube nanocomposites via liquid deposition modeling, Compos. Part A Appl. Sci. Manuf. 76 (2015) 110–114, https://doi.org/10.1016/j.compositesa.2015.05.014.
[7] C. Thibaut, Development of Fibrous Cellulosic Materials for the Production of Bio-Based 3D Printed Objects by Extrusion, Université Grenoble Alpes [2020-..], 2020. https://theses.hal.science/tel-02570560v1.
[8] T. Ma, L. Lv, C. Ouyang, X. Hu, X. Liao, Y. Song, X. Hu, Rheological behavior and particle alignment of cellulose nanocrystal and its composite hydrogels during 3D printing, Carbohydr. Polym. 253 (2021) 117217, https://doi.org/10.1016/j.carbpol.2020.117217.
[9] P.A. Amorim, M.A. d'Ávila, R. Anand, P. Moldenaers, P. Van Puyvelde, V. Bloemen, Insights on shear rheology of inks for extrusion-based 3D bioprinting, Bioprinting 22 (2021) e00129, https://doi.org/10.1016/j.bprint.2021.e00129.
[10] Q. Shi, K. Yu, X. Kuang, X. Mu, C.K. Dunn, M.L. Dunn, T. Wang, H. Jerry Qi, Recyclable 3D printing of vitrimer epoxy, Mater. Horiz. 4 (2017) 598–607, https://doi.org/10.1039/c7mh00043j.
[11] J.M. Capannelli, S. Dalle Vacche, A. Vitale, K. Bouzidi, D. Beneventi, R. Bongiovanni, A biobased epoxy vitrimer/cellulose composite for 3D printing by liquid deposition modelling, Polym. Test. 127 (2023) 108172, https://doi.org/10.1016/j.polymertesting.2023.108172.
[12] T. Vidil, F. Tournilhac, S. Musso, A. Robisson, L. Leibler, Control of reactions and network structures of epoxy thermosets, Prog. Polym. Sci. 62 (2016) 126–179, https://doi.org/10.1016/j.progpolymsci.2016.06.003.
[13] C. Lambré, J.M. Barat Baviera, C. Bolognesi, A. Chesson, P.S. Cocconcelli, R. Crebelli, D.M. Gott, K. Grob, E. Lampi, M. Mengelers, A. Mortensen, G. Rivière, V. Silano, I.L. Steffensen, C. Tlustos, L. Vernis, H. Zorn, M. Batke, M. Bignami, E. Corsini, R. FitzGerald, U. Gundert-Remy, T. Halldorsson, A. Hart, E. Ntzani, E. Scanziani, H. Schroeder, B. Ulbrich, D. Waalkens-Berendsen, D. Woelfle, Z. Al Harraq, K. Baert, M. Carfì, A.F. Castoldi, C. Croera, H. Van Loveren, Re-evaluation of the risks to public health related to the presence of bisphenol a (BPA) in foodstuffs, EFSA J. 21 (2023) e06857, https://doi.org/10.2903/j.efsa.2023.6857.
[14] P. Ares-Elejoste, R. Seoane-Rivero, I. Gandarias, A. Iturmendi, K. Gondra, Sustainable alternatives for the development of thermoset composites with low environmental impact, Polymers (Basel) 15 (2939) (2023) 1–16, https://doi.org/10.3390/polym15132939.
[15] F. Jaillet, E. Darroman, A. Ratsimihety, R. Auvergne, B. Boutevin, S. Caillol, New biobased epoxy materials from cardanol, Eur. J. Lipid Sci. Technol. 116 (2014) 63–73, https://doi.org/10.1002/ejlt.201300193.
[16] C. Voirin, S. Caillol, N.V. Sadavarte, B.V. Tawade, B. Boutevin, P.P. Wadgaonkar, Functionalization of cardanol: towards biobased polymers and additives, Polym. Chem. 5 (2014) 3142–3162, https://doi.org/10.1039/c3py01194a.
[17] R.S. Gour, V.V. Kodgire, M.V. Badiger, Toughening of epoxy novolac resin using cardanol based flexibilizers, J. Appl. Polym. Sci. 133 (2016), https://doi.org/10.1002/app.43318.
[18] P. Jia, F. Song, Q. Li, H. Xia, M. Li, X. Shu, Y. Zhou, Recent development of cardanol based polymer materials-a review, J Renew Mater 7 (2019) 601–619, https://doi.org/10.32604/jrm.2019.07011.
[19] I.C. Nwuzor, J.L. Chukwuneke, C.M. Ewulonu, P.C. Okolie, Fabrication of cardanol thermosetting resin reinforced with cellulose nanofibril/expanded graphite nano-biocomposites, Ind. Crop. Prod. 187 (2022) 115392, https://doi.org/10.1016/j.indcrop.2022.115392.
[20] Y. Hu, S. Tong, Y. Sha, J. Yu, L. Hu, Q. Huang, P. Jia, Y. Zhou, Cardanol-based epoxy vitrimer/carbon fiber composites with integrated mechanical, self-healing, reprocessable, and welding properties and degradability, Chem. Eng. J. 471 (2023) 144633, https://doi.org/10.1016/j.cej.2023.144633.
[21] S. Guggari, F. Magliozzi, S. Malburet, A. Graillot, M. Destarac, M. Guerre, Vanillin-based epoxy Vitrimers: looking at the Cystamine hardener from a different perspective, ACS Sustain. Chem. Eng. 11 (2023) 6021–6031, https://doi.org/10.1021/acssuschemeng.3c00379.
[22] P. Verdugo, D. Santiago, S. De la Flor, À. Serra, A biobased epoxy Vitrimer with dual relaxation mechanism: a promising material for renewable, Reusable, and Recyclable Adhesives and Composites, ACS Sustain Chem Eng 12 (2024) 5965–5978, https://doi.org/10.1021/acssuschemeng.4c00205.
[23] S. Tripathi, H. Supriya, S. Bose, Covalent adaptable network offers "sustainable" closed-loop circularity in epoxy vitrimers, SPE Polymers (2023), https://doi.org/10.1002/pls2.10113.
[24] S. Maes, N. Badi, J.M. Winne, F.E. Du Prez, Taking dynamic covalent chemistry out of the lab and into reprocessable industrial thermosets, Nat. Rev. Chem. 9 (2025) 144–158, https://doi.org/10.1038/s41570-025-00686-7.
[25] A. Sharma, A. Chand, I. Singh, B. Gaur, Vitrimers for 3D printing technology: current status and future perspectives, Ind. Eng. Chem. Res. 64 (2025) 2491–2515, https://doi.org/10.1021/acs.iecr.4c03705.
[26] B. Krishna Kumar, T.J. Dickens, Dynamic bond exchangeable thermoset vitrimers in 3D-printing, J. Appl. Polym. Sci. 140 (2023) e53304, https://doi.org/10.1002/app.53304.
[27] A. M'Barki, L. Bocquet, A. Stevenson, Linking rheology and printability for dense and strong ceramics by direct ink writing, Sci. Rep. 7 (2017) 6017, https://doi.org/10.1038/s41598-017-06115-0.

[28] U. Bodenschatz, M. Rosenthal, 3D printing of a wood-based furniture element with liquid deposition modeling, European Journal of Wood and Wood Products 82 (2024) 241–244, https://doi.org/10.1007/s00107-023-01996-7.
[29] A. Alhelal, Z. Mohammed, S. Jeelani, V.K. Rangari, 3D printing of spent coffee ground derived biochar reinforced epoxy composites, J. Compos. Mater. 55 (2021) 3651–3660, https://doi.org/10.1177/00219983211002237.
[30] C. Gauss, K.L. Pickering, L.P. Muthe, The use of cellulose in bio-derived formulations for 3D/4D printing: a review, Composites Part C: Open Access 4 (2021) 100113, https://doi.org/10.1016/j.jcomc.2021.100113.
[31] J. Lu, P. Askeland, L.T. Drzal, Surface modification of microfibrillated cellulose for epoxy composite applications, Polymer (Guildf) 49 (2008) 1285–1296, https://doi.org/10.1016/j.polymer.2008.01.028.
[32] P. Stenstad, M. Andresen, B.S. Tanem, P. Stenius, Chemical surface modifications of microfibrillated cellulose, Cellulose 15 (2008) 35–45, https://doi.org/10.1007/s10570-007-9143-y.
[33] J. Shojaeiarani, D.S. Bajwa, S. Chanda, Cellulose nanocrystal based composites: a review, Composites Part C: Open Access 5 (2021) 100164, https://doi.org/10.1016/j.jcomc.2021.100164.
[34] H. Seddiqi, E. Oliaei, H. Honarkar, J. Jin, L.C. Geonzon, R.G. Bacabac, J. Klein-Nulend, Cellulose and its derivatives: towards biomedical applications, Cellulose 28 (2021) 1893–1931, https://doi.org/10.1007/s10570-020-03674-w.
[35] A. Turbak, F. Snyder, R. Sandberg, Microfibrillated Cellulose US4374702A, 1983.
[36] I. Siró, D. Plackett, Microfibrillated cellulose and new nanocomposite materials: a review, Cellulose 17 (2010) 459–494, https://doi.org/10.1007/s10570-010-9405-y.
[37] P.A. Larsson, A.V. Riazanova, G. Cinar Ciftci, R. Rojas, H.H. Øvrebø, L. Wågberg, L. A. Berglund, Towards optimised size distribution in commercial microfibrillated cellulose: a fractionation approach, Cellulose 26 (2019) 1565–1575, https://doi.org/10.1007/s10570-018-2214-4.
[38] Production of microfibrillated cellulose fibers and their application in polymeric composites, in: M. Liu, K.G. Hoffmann, T. Geiger, G. Nyström, Elsevier Inc (Eds.), Nanotechnology in Paper and Wood Engineering: Fundamentals, Elsevier, Challenges and Applications, 2022, pp. 197–229, https://doi.org/10.1016/B978-0-323-85835-9.00003-9.
[39] C. Fu, C. Lin, W. Zhang, Y. Lin, J. Xiu, Y. Ni, L. Huang, Preparation of micro-fibrillated cellulose fibers by a simple two-step refining process for paper- based flexible electronic devices, Chem. Eng. J. 468 (2023) 143516, https://doi.org/10.1016/j.cej.2023.143516.
[40] M.-Andree. Wolf, Rana. Pant, Kirana. Chomkhamsri, Serenella. Sala, David. Pennington, The International Reference Life Cycle Data System (ILCD) Handbook - towards More Sustainable Production and Consumption for a Resource-Efficient Europe, Publications Office of the European Union, Luxembourg, 2012, https://doi.org/10.2788/85727.
[41] Carla. Caldeira, L.R.. Farcal, Irantzu. Garmendia Aguirre, Lucia. Mancini, Davide. Tosches, Antonio. Amelio, Kirsten. Rasmussen, Hubert. Rauscher, Juan. Riego Sintes, Serenella. Sala, Safe and sustainable by design chemicals and materials - Framework for the definition of criteria and evaluation procedure for chemicals and materials, in: EUR 31100 EN, Publications Office of the European Union, Luxembourg, 2022, https://doi.org/10.2760/487955.
[42] S. Manfredi, K. Allacker, K. Chomkhamsri, N. Pelletier, D. Maia De Souza, Product environmental footprint (PEF) guide, Joint Research Centre 873782 (2012) 1–154.
[43] ASTM International, Environmental management - life cycle assessment - principles and framework, BS EN ISO 14040:2006+A1:2020, Brussels, 2020.
[44] The British standards institution, Environmental management - life cycle assessment - requirements and guidelines, BS EN ISO 14044:2006+A2:2020, Brussels, 2021.
[45] T. Alsamad, M. Almazrouei, M.N. Hussain, I. Janajreh, Modeling of thermochemical conversion of glycerol: pyrolysis and H2O and CO2 gasification, Waste Biomass Valoriz. 9 (2018) 2361–2371, https://doi.org/10.1007/s12649-018-0306-x.
[46] V.Y. Mena-Cervantes, Raúl Hernández-Altamirano, A. Tiscareño-Ferrer, Development of a green one-step neutralization process for valorization of crude glycerol obtained from biodiesel, ADVANCES IN ENVIRONMENTAL BIOTECHNOLOGY AND ENGINEERING (2018), https://doi.org/10.1007/s11356-019-07287-0/Published.
[47] 聂强杨国岭, Preparation Method of High-Content Cysteamine Hydrochloride, CN 109503441 B, 2018.
[48] M. Temmerman, P.D. Jensen, J. Hébert, Von Rittinger theory adapted to wood chip and pellet milling, in a laboratory scale hammermill, Biomass Bioenergy 56 (2013) 70–81, https://doi.org/10.1016/j.biombioe.2013.04.020.
[49] E. Albertini, S. Dalle Vacche, R. Bongiovanni, I. Bianco, G.A. Blengini, A. Vitale, Biobased and Reprocessable Vitrimers based on Cardanol-derived epoxy for more sustainable thermosets, ACS Sustain. Chem. Eng. (2025), https://doi.org/10.1021/acssuschemeng.4c09035.
[50] H. Barbara, Stuart, Infrared Spectroscopy : Fundamentals and Applications, John Wiley & Sons, Ltd, Sydney, 2004.
[51] M. González González, J.C. Cabanelas, J. Baselga, Applications of FTIR on epoxy resins - identification, monitoring the curing process, phase separation and water uptake, in: Theophile Theophanides (Ed.), Infrared Spectroscopy – Materials Science, Engineering and Technology, IntechOpen, 2012, pp. 261–284, https://doi.org/10.5772/2055.
[52] E. Fortunati, M. Peltzer, I. Armentano, L. Torre, A. Jiménez, J.M. Kenny, Effects of modified cellulose nanocrystals on the barrier and migration properties of PLA nano-biocomposites, Carbohydr. Polym. 90 (2012) 948–956, https://doi.org/10.1016/j.carbpol.2012.06.025.
[53] L. Kang, P. Chen, B. Wang, J. Jia, J. Li, J. Zeng, Z. Cheng, W. Gao, J. Xu, K. Chen, Cellulose nanocrystal dye as reinforcement matrix of lipstick for inhibiting color migration, Cellulose 27 (2020) 905–913, https://doi.org/10.1007/s10570-019-02827-w.
[54] W.H. Herschel, R. Bulkley, Konsistenzmessungen von Gummi-Benzollösungen, Kolloid-Zeitschrift 39 (1926) 291–300, https://doi.org/10.1007/BF01432034.
[55] E. Feilden, Additive manufacturing of ceramics and ceramic composites via robocasting, Centre for Advanced Structural Ceramics, Imperial College London (2017), https://doi.org/10.13140/RG.2.2.29343.25765.
[56] G. Williams, D.C. Watts, Non-symmetrical dielectric relaxation behaviour arising from a simple empirical decay function, Trans. Faraday Soc. 66 (1970) 80–85, https://doi.org/10.1039/TF9706600080.
[57] K.S. Fancey, A mechanical model for creep, recovery and stress relaxation in polymeric materials, J. Mater. Sci. 40 (2005) 4827–4831, https://doi.org/10.1007/s10853-005-2020-x.
[58] A. Duval, W. Benali, L. Avérous, Turning lignin into a recyclable bioresource: transesterification vitrimers from lignins modified with ethylene carbonate, Green Chem. 26 (2024) 8414–8427, https://doi.org/10.1039/d4gc00567h.
[59] L. Li, X. Chen, K. Jin, J.M. Torkelson, Vitrimers designed both to strongly suppress creep and to recover original cross-link density after reprocessing: quantitative theory and experiments, Macromolecules 51 (2018) 5537–5546, https://doi.org/10.1021/acs.macromol.8b00922.
[60] Y. Spiesschaert, C. Taplan, L. Stricker, M. Guerre, J.M. Winne, F.E. Du Prez, Influence of the polymer matrix on the viscoelastic behaviour of vitrimers, Polym. Chem. 11 (2020) 5377–5385, https://doi.org/10.1039/d0py00114g.
[61] A.E. Krauklis, A.T. Echtermeyer, Mechanism of yellowing: carbonyl formation during hygrothermal aging in a common amine epoxy, Polymers (Basel) 10 (2018) 1017, https://doi.org/10.3390/polym10091017.